Autonomous Synchronizing and Frequency Response Control of Multi-terminal DC Systems with Wind Farm Integration

Renxin Yang, *Student Member*, *IEEE*, Gang Shi, *Member*, *IEEE*, Xu Cai, Chen Zhang, Gen Li, *Member*, *IEEE*, Jun Liang, *Senior Member*, *IEEE*.

***Abstract*—Recent analyses have shown that the grid-integration of offshore wind farms through MTDC systems has brought low inertia and small-signal stability issues, in which the dynamics of phase-locked-loop (PLL) play a crucial role. To address this issue, this paper proposes a control strategy for the multi-terminal VSCs aiming at PLL-less synchronization and autonomous frequency response of the MTDC system. One of the significant features of the proposed control is that the deviation of the grid frequency can be instantaneously reflected on the deviation of the DC voltage without ancillary control. Based on this feature, a fast inertia response and primary frequency regulation among wind farms and AC systems interconnected by the MTDC system can be achieved. A small-signal model is established to evaluate the overall system stability using the proposed control. Finally, comparative studies of this proposed control with the conventional PLL-based vector control are conducted in PSCAD/EMTDC based on a practical MTDC system in China, the Zhangbei four-terminal HVDC transmission system. The analysis shows that the proposed control exhibits advantages in weak grid operation and autonomous frequency response.**

***Index Terms*—frequency response, weak grid, wind farms, inertia, MMC MTDC, small signal stability analysis**

NOMENCLATURE

C_{eq}	Equivalent DC capacitance
U_{dc}	DC voltage
U_{dc_nom}	Nominal DC voltage
P_{dc}	DC side active power of receiving end converter (REC)
P_{ac}	AC side active power of the REC
Q_{ac}	AC side reactive power of the REC
U_{rec}	AC voltage of REC
ω_{rec}	AC frequency of REC
ω_{nom}	Nominal frequency
J	Moment of inertia
ω_m	Rotor speed of synchronous generator (SG)
P_m	Mechanical power input of SG
ω_e	AC frequency of SG
P_e	Active power output of SG
p	Polar pairs
K	Coupling coefficient
ω_g	AC grid frequency
δ	Power angle
m	Modulation ratio of REC
X	Equivalent grid impedance
P_0	Steady-state operating point of P_{ac}
δ_0	Steady-state operating point of δ
U_{dc_ref}	Reference DC voltage of REC
P_{ref}	Reference active power of REC
Q_{ref}	Reference reactive power of REC
D	Droop coefficient
θ	Phase angle of REC AC voltage
ω_{WF}	Frequency of AC bus for wind farm collection
ω_{WT}	Rotor speed of the wind turbine
N_{dc}	Proportion between wind farm collection AC bus frequency deviation and DC voltage deviation
P_{WF_nom}	Nominal wind power
P_{add}	Additional wind power
T_p	Time constant of the wind turbine's power loop
T_{filter}	Time constant of the filter in sending end converter
i_{jk}	DC line currents between port j and k
L_{jk}	DC line reactance between port j and k
C_j	Equivalent capacitance of port j
U_j	DC voltage of port j

I. Introduction

In order to deliver electric power from different places over long-distance, multi-terminal high-voltage direct current (MTDC) system is a promising solution [1]-[2] and becomes a trend for the grid-integration of offshore wind farms [3]-[4]. However, the growing wind power penetration with the adoption of MTDC systems has brought challenges in grid operations, e.g., the low inertia and small-signal stability issues, which are still under-researched.

Due to the isolation of MTDC systems, wind farms can hardly sense the grid frequency variation [5]. This may have a negative impact on the frequency stability of AC grids since the wind farms basically provide no inertia response and primary

This work is supported by the National Natural Science Foundation of China under Grant 51677117. (*Corresponding authors: Xu Cai and Gang Shi*)

Renxin Yang, Gang Shi, Xu Cai are with the Key Laboratory of Control of Power Transmission and Conversion, Ministry of Education, Shanghai Jiao Tong University, Shanghai, 200240, China. (Emails: {frank_yang; gangshi; xucai}@sjtu.edu.cn)

Chen Zhang is with the Department of Engineering Cybernetics, Norwegian University of Science and Technology, 7034, Trondheim, Norway (Email: chen.zhang@ntnu.no)

Gen Li and Jun Liang are with School of Engineering, Cardiff University, Cardiff, CF24 3AA, Wales, UK (Emails: {LiG9; LiangJ1}@cardiff.ac.uk)

frequency regulation under such circumstances. In order to address this issue, authors of [6] employ a centralized communication and master-slave control for MTDC systems. The output power of wind farms and receiving end converters (RECs) are regulated according to grid frequency variations dispatched through the centralized communication. However, the cost and reliability of long-distance communication are the main challenges for this method. Therefore, a communication-less strategy is preferred and has been proposed in [7]-[9], where the extra *P-f* droop control is attached to the conventional *P*-U_{dc} droop control in MTDC grids. Based on the *P-f* and *P*-U_{dc} droop controls of the MTDC system, AC power systems of different terminals can sense frequency variations occurred in one of the AC systems and provide frequency support. Furthermore, a linear relationship between grid frequency variations and DC voltage deviations is established in [10]. Based on this method, sending-end-converters (SECs) can adjust the AC frequency by detecting the DC voltage deviation. This feature can facilitate the realization of wind farm frequency support.

Another emerging problem may be encountered with MTDC systems is the small-signal stability. This is because RECs of an MTDC system usually employ the conventional grid-feeding control strategy of voltage source converters (VSCs), where the phase-locked-loop (PLL) is utilized for grid synchronization and current vector control. This control has been proven sensitive to grid impedance variations, and if the control parameters are not properly designed, it may lead to oscillations particularly under a weak grid condition [11]-[12], i.e., a low short-circuit-ratio (SCR). More importantly, some analyses have shown that the PLL plays a significant role in such stability issues [13]-[14]. Therefore, a PLL-less control of VSC is attractive from this point of view, e.g. the virtual synchronous generator (VSG) control [15]-[16], which performs well even under weak grid conditions and has the capability to provide inertia response autonomously. Application of the VSG concept in the controls of VSC-MTDC grids is not a trivial issue due to the complexity. Recent work has been proposed in [17] where an outer U_{dc}-*P* droop control is added to achieve autonomous power-sharing. However, this control scheme is a cascaded control structure with multiple loops which is complicated and therefore is difficult to tune the parameters. More importantly, the outer loop control bandwidth may not be sufficient for a VSC with low switching frequency.

In order to reduce the complexity of the VSG control of VSCs, recently, a novel concept of PLL-less grid synchronization by directly using the intrinsic dynamic of the DC-link voltage has been proposed in [18] and [19]. Moreover, the DC voltage dynamic is inherently bound with the AC frequency variation with this control concept. This U_{dc}-*f* droop characteristic is first explored in [20], yet, it is only tested in a point-to-point VSC-HVDC link. In [21], this feature is utilized in a point-to-point VSC-HVDC link to facilitate the inertia response of wind farms. However, few studies have been done on the development and application of this concept to the control of MTDC systems with wind farm integration. In this situation, there exists the need for autonomous power-sharing among RECs. Moreover, autonomous primary frequency regulation among multiple RECs and communication-less inertia response from wind farms can be realized to enhance the frequency stability of the onshore AC grids.

To bridge this gap, this paper proposes a coordinated control strategy for MTDC systems with wind farm integration, including a PLL-less control utilizing DC-link voltage dynamic for single REC and the autonomous power-sharing and primary frequency regulation among multiple RECs utilizing DC droop characteristics. The proposed control strategy also benefits for the communication-less inertia response control of wind farms with the coordination of SECs. Salient features can be achieved with the proposed control strategy: being robust to grid impedance changes and being capable to provide fast auxiliary services, i.e., primary frequency regulation and inertia response. Therefore, both low inertia and small-signal stability issues are solved.

The remainder of this paper is organized as follows. The introduction of a practical four-terminal MTDC system with wind farm integration and the basic principles of the PLL-less control strategy are presented in Section II. The power-sharing and primary frequency regulation characteristics of the multiple RECs, and the inertia response control of wind farms are revealed and analyzed in Section III. In Section IV, system stability is studied by analyzing the eigenvalues for different parameters. Simulation results are shown in Section V. Conclusions are drawn in Section VI.

II. Autonomous-synchronizing Control of RECs with DC droop Characteristic

A. System description

This paper is going to base the analysis on a practical MTDC system in China, which is the Zhangbei four-terminal HVDC system. As shown in Fig. 1, the Zhangbei four-terminal HVDC system is a ±500 kV bipolar meshed MTDC network with wind farm integrations as well as synchronous AC grids. The wind turbines are with full-scale power converters, and only the positive pole is studied as the two poles are symmetric.

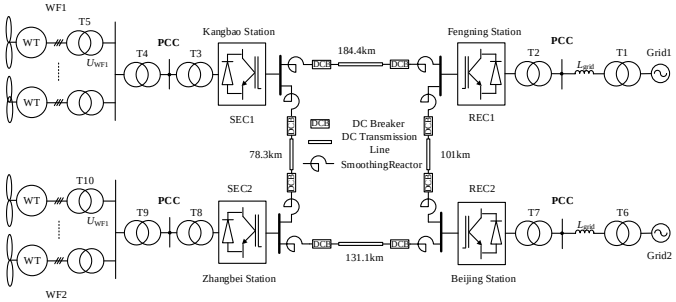

Fig. 1. An MTDC system with wind farm and synchronous AC grid integration.

B. Self-synchronizing Control Using DC Capacitor Inertia

Fig. 2 is the typical topology of a REC. C_{eq} is the DC side equivalent capacitor. For the modular multilevel converter (MMC) utilized in the studied system, C_{eq} is the equivalent DC capacitor of all sub-module (SM) capacitors. The input power P_{dc} from the DC grid can be regulated by adjusting U_{dc}. The output power P_{ac} to the AC grid can be varied by changing U_{rec} and ω_{rec}, i.e., the three-phase AC voltage and frequency.

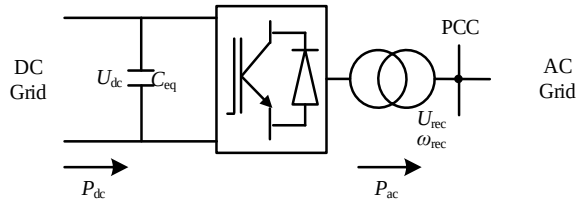

Fig. 2. A typical topology of the REC station.

The DC voltage dynamic can be written as :

$$C_{eq}U_{dc}\frac{dU_{dc}}{dt}=P_{dc}-P_{ac}. \quad (1)$$

Therefore, the deviation of the input power from the DC grid and the output power to the AC grid will be directly reflected on the DC voltage, which is very similar to the rotor equation of the SG:

$$J\omega_m\frac{d\omega_m}{dt}=P_m-P_e. \quad (2)$$

For an SG, the power angle and the output active power P_e will decrease when its output frequency ω_e doesn't synchronize with the grid, e.g., smaller than the grid frequency. Then the left side of (2) becomes positive, and the rotor speed ω_m will increase. Since there is a natural equation between ω_m and ω_e:

$$\omega_m = p\omega_e, \quad (3)$$

ω_e will increase to the same as the grid frequency. This is the self-synchronizing principle of the SG. It can be found the only difference between the REC and SG is the absence of (3). Therefore, a relationship between the AC frequency of REC and the DC voltage is established in the proposed control strategy:

$$\frac{U_{dc}-U_{dc\_nom}}{U_{dc\_nom}}=K\frac{\omega_{rec}-\omega_{nom}}{\omega_{nom}}. \quad (4)$$

Then the REC will achieve the self-synchronizing characteristic like an SG, i.e., the following correlation can be established:

$$\omega_g\uparrow\Rightarrow\delta\downarrow\Rightarrow P_{ac}\downarrow\Rightarrow U_{dc}\uparrow\Rightarrow\omega_{rec}\uparrow. \quad (5)$$

By using the intrinsic inertia of the DC-link equivalent capacitor, self-synchronizing is achieved in the REC. The negative influence of using the PLL to track the grid phase angle is avoided.

C. Grid Frequency Tracking Characteristic of DC Voltage

The output equation of the REC is given below:

$$\begin{cases} P_{ac}=\dfrac{3U_{rec}U_g}{X}\sin\delta\approx\dfrac{3mU_{dc}U_g}{2\sqrt{2}X}\delta \\ \dfrac{d\delta}{dt}=\omega_{rec}-\omega_g \end{cases}. \quad (6)$$

After linearization at the operating point, (7) can be derived by the substitution of (6) and (4) into (1):

$$\Delta P_{dc}=C_{eq}U_{dc\_nom}\frac{d(U_{dc}-U_{dc\_nom})}{dt}+\frac{P_0(U_{dc}-U_{dc\_nom})}{U_{dc\_nom}}+\frac{P_0}{\delta_0}\int\left(\frac{U_{dc}-U_{dc\_nom}}{KU_{dc\_nom}}\omega_{nom}-\Delta\omega_g\right). \quad (7)$$

Assuming that the active power at DC side remains constant, i.e., $\Delta P_{dc} = 0$, there is:

$$\begin{cases} \dfrac{U_{dc}\text{-}U_{dc\_nom}}{U_{dc\_nom}}=K\dfrac{\omega_{rec}-\omega_{nom}}{\omega_{nom}}=G(s)K\dfrac{\omega_g-\omega_{nom}}{\omega_{nom}} \\ G(s)=\dfrac{\dfrac{1}{K}}{\dfrac{C_{eq}U_{dc\_nom}^2\delta_0}{P_0\omega_{nom}}s^2+\dfrac{\delta_0}{\omega_{nom}}s+\dfrac{1}{K}} \end{cases}. \quad (8)$$

The value of K is set as 5. Taking the parameters of Fengning station (REC2) as an example, which can be found in Table I of Section IV, the bode diagram of G(s) is shown in Fig. 3.

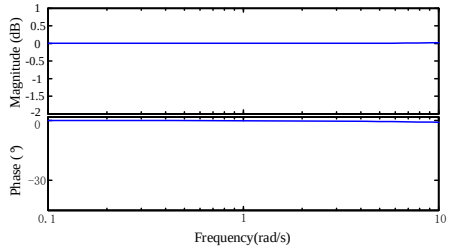

Fig. 3. Bode diagram of the transfer function G(s).

The process of a grid's typical inertia response usually lasts for 6 s. Assuming that the grid frequency changes exponentially, the time constant of this process is about 1.5 s, which corresponds to a cut-off frequency of 0.67rad/s. It can be observed from Fig. 3 that the amplitude of G(s) is 1 and the phase delay of G(s) is nearly 0 ° around 0.67rad/s. Therefore, the DC voltage and the REC output frequency can be considered to track grid frequency variation in real-time.

D. DC Voltage Droop Control

When the proposed strategy is utilized, it can be observed from (8) that the DC voltage of REC will be locked if the AC grid frequency is constant. Therefore, this method cannot be directly applied to the MTDC system, since the power flow will become uncontrollable if the DC voltages of RECs are identical.

In order to solve this problem, a DC voltage droop should be added to the control loop. In the left side of (4), U_{dc_nom} in the numerator is replaced by U_{dc_ref}, which is:

$$\begin{cases} \dfrac{U_{dc}\text{-}U_{dc\_ref}}{U_{dc\_nom}}=K\dfrac{\omega_{rec}-\omega_{nom}}{\omega_{nom}} \\ U_{dc\_ref}=U_{dc\_nom}+(P_{ac}-P_{ref})\times D \end{cases}. \quad (9)$$

The droop coefficient D will determine the power allocation of multiple RECs. Next, the power-sharing mechanism resulting from the droop control of multi-terminal VSCs and the frequency response from wind farms will be analyzed.

III. Power-sharing Mechanism and Frequency Response of the MTDC System

A. Simplified Model of the 4-Terminal HVDC System

This section focuses on the steady-state power flow of the MTDC system and wind farms. Therefore, the output active power of wind farms is considered to be constant, so is the output active power of SECs. As for RECs with the proposed control strategy, the dynamics of $G(s)$ are neglected, i.e., $G(s) = 1$. According to (8), there is:

$$\frac{U_{dc}-U_{dc\_ref}}{U_{dc\_nom}}=K\frac{\omega_g-\omega_{nom}}{\omega_{nom}}. \quad (10)$$

The four-terminal MTDC system in Fig. 1 is simplified as below in Fig. 4. Because the virtual resistance brought by the droop control is usually much larger, the influence of the transmission line resistance is neglected when considering steady-state power allocation. The DC voltages of REC1 and REC2 are nearly the same and therefore can be considered as one value.

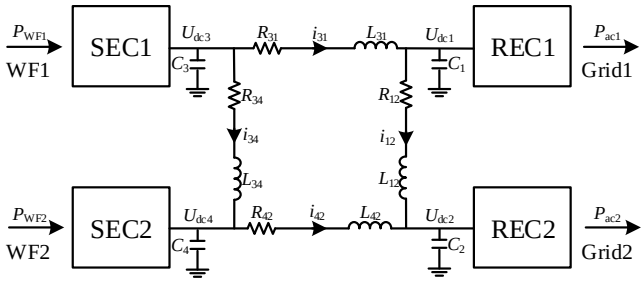

Fig. 4. A simplified model of the MTDC system.

Substituting (10) into (9), the control of RECs can be expressed as:

$$\begin{cases} U_{dc}=\dfrac{K_i U_{dc\_nom}}{\omega_{nom}}\Delta\omega_{gi}+(P_{aci}-P_{refi})D_i+U_{dc\_nom} \\ P_{aci}=P_{refi}+\dfrac{1}{D_i}(U_{dc}-U_{dc\_nom}-\dfrac{K_i U_{dc\_nom}}{\omega_{nom}}\Delta\omega_{gi}) \\ \forall i\in(1,\ 2) \end{cases}. \quad (11)$$

During normal operation, the frequency variation $\Delta\omega_{gi}$ of the power grid is zero. The active power deviation $P_{aci} - P_{refi}$ of the REC is inversely proportional to the droop coefficient D_i.

B. Primary Frequency Regulation from the MTDC System

Neglecting the power losses on the transmission line, (12) can be observed from Fig. 4:

$$P_{WF}=P_{WF1}+P_{WF2}=P_{ac1}+P_{ac2}. \quad (12)$$

Substituting of (11) into (12) yields:

$$P_{WF}-(P_{ref1}+P_{ref2})=(\frac{1}{D_1}+\frac{1}{D_2})(U_{dc}-U_{dc\_nom})- \frac{U_{dc\_nom}}{\omega_{nom}}(\frac{K_1}{D_1}\Delta\omega_{g1}+\frac{K_2}{D_2}\Delta\omega_{g2}) \quad (13)$$

(13) can be rearranged as:

$$U_{dc}-U_{dc\_nom}=\frac{\Delta P+\frac{U_{dc\_nom}}{\omega_{nom}}(\frac{K_1}{D_1}\Delta\omega_{g1}+\frac{K_2}{D_2}\Delta\omega_{g2})}{\frac{1}{D_1}+\frac{1}{D_2}}, \quad (14)$$

where $\Delta P = P_{WF} - (P_{ref1} + P_{ref2})$.

Substituting (14) into (11), the output power of REC 1 and 2 are:

$$\begin{cases} P_{ac1}=P_{ref1}+\dfrac{\Delta P+\frac{U_{dc\_nom}}{\omega_{nom}}(K_2\Delta\omega_{g2}-K_1\Delta\omega_{g1})}{D_1+D_2} \\ P_{ac2}=P_{ref2}+\dfrac{\Delta P+\frac{U_{dc\_nom}}{\omega_{nom}}(K_1\Delta\omega_{g1}-K_2\Delta\omega_{g2})}{D_1+D_2} \end{cases}. \quad (15)$$

Assuming there is a frequency deviation $\Delta\omega_{g1}$ in Grid 1, the power variation caused by $\Delta\omega_{g1}$ is:

$$\Delta P_{ac1}=-\Delta P_{ac2}=-\frac{U_{dc\_nom}}{\omega_{nom}}\frac{K_1}{D_1+D_2}\Delta\omega_{g1}. \quad (16)$$

And if the grid frequency variation occurs in Grid 2, the power variation will be:

$$\Delta P_{ac2}=-\Delta P_{ac1}=-\frac{U_{dc\_nom}}{\omega_{nom}}\frac{K_2}{D_1+D_2}\Delta\omega_{g2}. \quad (17)$$

It can be observed from (16) and (17) that the MTDC system will regulate the active power among multiple RECs to provide frequency support to the grid in which frequency variation occurs. The amplitude of the additional power is proportional to the frequency deviation $\Delta\omega_{gi}$. Therefore, autonomous primary frequency regulation can be realized with the proposed control strategy.

C. Inertia Support from Wind Farms

According to (14), the frequency deviation of both Grids 1 and 2 can be reflected on the HVDC bus voltage:

$$\Delta U_{dc}=\frac{U_{dc\_nom}}{\omega_{nom}}(\frac{\frac{K_1}{D_1}\Delta\omega_{g1}+\frac{K_2}{D_2}\Delta\omega_{g2})}{\frac{1}{D_1}+\frac{1}{D_2}}. \quad (18)$$

It can be seen from (18) that ΔU_{dc} is the weighted sum of $\Delta\omega_{g1}$ and $\Delta\omega_{g1}$. The weighting factors are K_1/D_1 and K_2/D_2.

Therefore, SECs can be informed with grid frequency variations by detecting the DC voltage. The frequency information is transferred to wind farms by regulating its AC frequency. The relationship between the detected DC bus voltages and output frequency references of SECs are shown below:

$$\Delta\omega_{WFi}=N_{dc}\frac{\omega_{nom}}{U_{dc\_nom}}\Delta U_{dc}. \quad (19)$$

Since the maximum DC voltage deviation is usually ±5%, and the maximum frequency deviation of the wind farm collection AC bus is usually ±0.5Hz (1%), (20) can be derived from (19):

$$1\% \geq 5\% N_{dc}. \quad (20)$$

In this paper, N_{dc} is set to 0.2 to maximize the accuracy of obtaining grid frequency.

Hence, the frequency variations of AC grids are reflected in the output frequency of SECs, which can be sensed by the wind turbines.

The capability of wind turbines to provide an inertia response is investigated in [22]-[24]. An additional value associated with the rate-of-change-of-frequency (ROCOF) is attached to the active power reference (P_{MPPT}) given by the MPPT control. The additional power P_{add} is provided by accelerating or decelerating the wind turbine and utilizing the kinetic energy stored in rotating blades. Assuming that the virtual inertia of a wind farm is H_{WF}, the value of P_{add} is:

$$\begin{cases} P_{\mathrm{addi}} = -2H_{\mathrm{WFi}} \dfrac{\mathrm{d}\omega_{\mathrm{WFi}}}{\mathrm{d}t} \dfrac{P_{\mathrm{WF\_nomi}}}{\omega_{\mathrm{nom}}} \\ \forall i \in (1,\ 2) \end{cases} . \tag{21}$$

The overall control diagram of the proposed coordinated control strategy is shown in Fig. 5. The control strategies of SEC1 and REC1 are the same as SEC2 and REC2, respectively.

U_{rec_abc} is the reference voltage for each phase of the REC. The phase angle θ of U_{rec_abc} is the integration of ω_{rec}. The relationship among U_{dc}, P_{ac} and ω_{rec} is mentioned in (9). The modulation ratio m, which decides the amplitude of U_{rec_abc}, is utilized to control the reactive power.

The control of SEC is similar to the control of REC apart from droop characteristics. However, SEC functions as an AC voltage source and presents no inertia due to the rapid current vector control of the grid-side converter of the wind turbine. In addition, only a single AC voltage loop is utilized in SECs, since there is no filter capacitor at the AC side of MMCs.

IV. Small-Signal Stability Analysis

In this section, a small-signal state-space model of the four-terminal MTDC system shown in Fig. 4 using the proposed control strategy will be established. Then, based on this model, overall system stability margin will be evaluated with different system parameters.

A. Small-Signal Model

The AC grid is modelled as a constant voltage source with a grid impedance. Only the active power loops of RECs are taken into consideration since the reactive power control is usually much slower. The state-space equations of P_{ac1} and P_{ac2} can be derived from (6):

$$\begin{cases} \dfrac{\mathrm{d}\Delta P_{\mathrm{aci}}}{\mathrm{d}t} = \dfrac{P_{\mathrm{aci0}}}{U_{\mathrm{dc0}}} \dfrac{\mathrm{d}\Delta U_{\mathrm{dc}}}{\mathrm{d}t} + \dfrac{P_{\mathrm{aci0}}}{\delta_{\mathrm{i0}}} \dfrac{\mathrm{d}\Delta\delta}{\mathrm{d}t} \\ \quad = \dfrac{P_{\mathrm{aci0}}}{U_{\mathrm{dci0}}} \dfrac{\mathrm{d}\Delta U_{\mathrm{dc}}}{\mathrm{d}t} + \dfrac{P_{\mathrm{aci0}}}{\delta_{\mathrm{i0}}} (\Delta\omega_{\mathrm{rec}} - \Delta\omega_{\mathrm{gi}}) \\ \quad = \dfrac{P_{\mathrm{aci0}}}{U_{\mathrm{dci0}}} \dfrac{\mathrm{d}\Delta U_{\mathrm{dc}}}{\mathrm{d}t} + \dfrac{P_{\mathrm{aci0}}}{\delta_{\mathrm{i0}}} \dfrac{\omega_{\mathrm{nom}}}{K_{\mathrm{i}} U_{\mathrm{dc\_nom}}} (\Delta U_{\mathrm{dc}} - D\Delta P_{\mathrm{aci}}) \\ \forall i \in (1,\ 2) \end{cases} , \tag{22}$$

where P_{aci0} and δ_{i0} are the steady-state values of P_{ac} and δ.

The linearized circuit equations are obtained in (23) where C_1~C_4 are the equivalent DC side capacitances of the converters, R_{31}, R_{34}, R_{42}, and R_{12} are the resistances of the transmission line, L_{31}, L_{34}, L_{42}, and L_{12} are the sum of smoothing reactance, line reactance, and MMC arm reactance. Since overhead lines are utilized in the Zhangbei system, the capacitances of transmission lines are neglected.

$$\begin{cases} \dfrac{\mathrm{d}\Delta i_{31}}{\mathrm{d}t} = \dfrac{1}{L_{31}} \left(\Delta U_{\mathrm{dc3}} - \Delta U_{\mathrm{dc1}} - R_{31}\Delta i_{31} \right) \\ \dfrac{\mathrm{d}\Delta i_{34}}{\mathrm{d}t} = \dfrac{1}{L_{12}} \left(\Delta U_{\mathrm{dc3}} - \Delta U_{\mathrm{dc4}} - R_{34}\Delta i_{34} \right) \\ \dfrac{\mathrm{d}\Delta i_{12}}{\mathrm{d}t} = \dfrac{1}{L_{12}} \left(\Delta U_{\mathrm{dc1}} - \Delta U_{\mathrm{dc2}} - R_{12}\Delta i_{12} \right) \\ \dfrac{\mathrm{d}\Delta i_{42}}{\mathrm{d}t} = \dfrac{1}{L_{42}} \left(\Delta U_{\mathrm{dc4}} - \Delta U_{\mathrm{dc2}} - R_{42}\Delta i_{42} \right) \end{cases} \begin{cases} \dfrac{\mathrm{d}\Delta U_{\mathrm{dc1}}}{\mathrm{d}t} = \dfrac{1}{C_1} \left(\Delta i_{31} - \Delta i_{12} - \Delta \dfrac{P_{\mathrm{ac1}}}{U_{\mathrm{dc1}}} \right) \\ \dfrac{\mathrm{d}\Delta U_{\mathrm{dc2}}}{\mathrm{d}t} = \dfrac{1}{C_2} \left(\Delta i_{42} + \Delta i_{12} - \Delta \dfrac{P_{\mathrm{ac2}}}{U_{\mathrm{dc2}}} \right) \\ \dfrac{\mathrm{d}\Delta U_{\mathrm{dc3}}}{\mathrm{d}t} = \dfrac{1}{C_3} \left(-\Delta i_{31} - \Delta i_{34} + \Delta \dfrac{P_{\mathrm{WF1}}}{U_{\mathrm{dc3}}} \right) \\ \dfrac{\mathrm{d}\Delta U_{\mathrm{dc4}}}{\mathrm{d}t} = \dfrac{1}{C_4} \left(-\Delta i_{42} + \Delta i_{34} + \Delta \dfrac{P_{\mathrm{WF2}}}{U_{\mathrm{dc4}}} \right) \end{cases} \tag{23}$$

As for SECs, the relationship between $\Delta\omega_{WF}$ and ΔU_{dc} is shown in (24), which can be derived from (19). The dynamics of ω_{WF} regulation is neglected since it usually lasts for only several switching cycles. In addition, a filter is used to filter out the noise of the DC voltage. The time constant of this filter is set to 0.2s, corresponding to a cut-off frequency of 5rad/s.

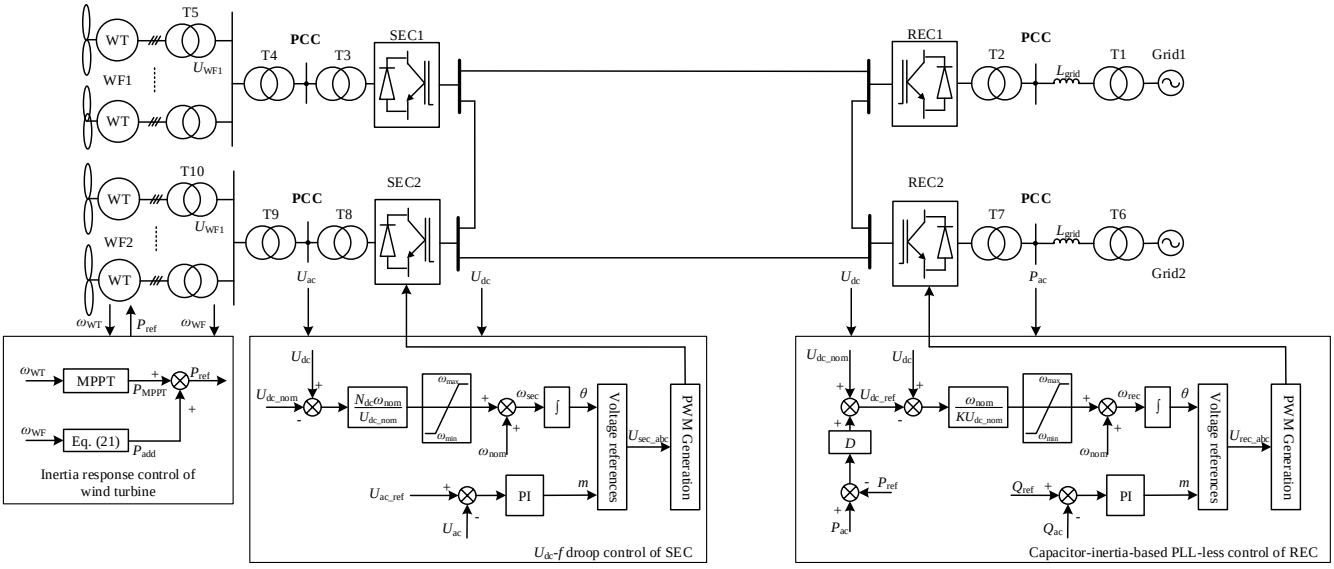

Fig. 5. The overall control diagram of the MTDC system and wind farms with the proposed control strategy.

$$\begin{cases} \Delta\omega_{\mathrm{WFi}} = \dfrac{1}{(1+T_{\mathrm{filter}}s)} \dfrac{N_{\mathrm{dc}}\omega_{\mathrm{nom}}}{U_{\mathrm{dc\_nom}}} \Delta U_{\mathrm{dci}} \\ \forall i \in (1,\ 2) \end{cases}. \tag{24}$$

In order to simplify the analysis, the wind farm is aggregated to a single wind turbine. Assuming that the wind power remains constant, ΔP_{WF1} and ΔP_{WF2} are determined by an additional power reference, ΔP_{add}:

$$\begin{cases} \Delta P_{\mathrm{WFi}} = \dfrac{1}{1+T_{\mathrm{p}}s} \Delta P_{\mathrm{addi}} \\ \forall i \in (1,\ 2) \end{cases}, \tag{25}$$

where T_{p} is the time constant of the wind turbine's power loop, which is usually 0.05s.

According to (21) and (24), ΔP_{add} is:

$$\begin{cases} \Delta P_{\mathrm{addi}} = -\dfrac{2H_{\mathrm{WFi}}P_{\mathrm{WF\_nomi}}}{\omega_{\mathrm{nom}}} \dfrac{\mathrm{d}\Delta\omega_{\mathrm{WFi}}}{\mathrm{d}t} = -\dfrac{2H_{\mathrm{WFi}}N_{\mathrm{dc}}P_{\mathrm{WF\_nomi}}}{(1+T_{\mathrm{filter}}s)U_{\mathrm{dc\_nom}}} \dfrac{\mathrm{d}\Delta U_{\mathrm{dci}}}{\mathrm{d}t} \\ \forall i \in (1,\ 2) \end{cases}. \tag{26}$$

The state-space equation of the system shown in Fig. 4 can be written as:

$$\boldsymbol{B}\dot{\boldsymbol{x}} = \boldsymbol{A}\boldsymbol{x} + \boldsymbol{C}\boldsymbol{u}\ , \tag{27}$$

where $\boldsymbol{x} = [\Delta U_{\mathrm{dc1}}\ \Delta U_{\mathrm{dc2}}\ \Delta U_{\mathrm{dc3}}\ \Delta U_{\mathrm{dc4}}\ \Delta i_{31}\ \Delta i_{34}\ \Delta i_{12}\ \Delta i_{42}\ \Delta P_{\mathrm{ac1}}\ \Delta P_{\mathrm{ac2}}\ \Delta P_{\mathrm{add1}}\ \Delta P_{\mathrm{add2}}\ \Delta P_{\mathrm{WF1}}\ \Delta P_{\mathrm{WF2}}]^{\mathrm{T}}$.

B. Small-Signal Analysis

The eigenvalues of the system transfer function can be calculated by solving:

$$\det\left[\lambda \boldsymbol{I}_{14} - \boldsymbol{B}^{-1} \times \boldsymbol{A}\right] = 0 \tag{28}$$

The distribution of eigenvalues is shown in Fig. 6. Some basic electrical parameters of the MTDC system are listed in Table I. The critical control parameters are shown in Table II, and their influence on system stability will be discussed in the following sections.

TABLE I
PARAMETERS OF THE MTDC SYSTEM

Parameters	Values
Rated DC voltage	500kV
Rated grid voltage (line-to-line)	260kV
Transformer leakage inductance	0.17 p.u.
REC1 and SEC1	
SM number	220
SM rated voltage	2.3kV
SM capacitance	7mF
Rated active power	750MW
Rated reactive power	0
Arm inductance	0.1 p.u.
REC2 and SEC2	
SM number	220
SM rated voltage	2.3kV
SM capacitance	14mF
Rated active power	1500MW
Rated reactive power	0
Arm inductance	0.1 p.u.
Transmission line	
Resistance	0.01273Ω/km
Capacitance	0.01274uF/km
Reactance	0.9337mH/km
DC line reactor	200mH

TABLE II
CRITICAL PARAMETERS

Symbols	Values
H_{WF1}	3
H_{WF2}	3
D_1	1/30
D_2	1/60
K_1	1
K_2	2
SCR_1	10
SCR_2	10
N_{dc}	0.2

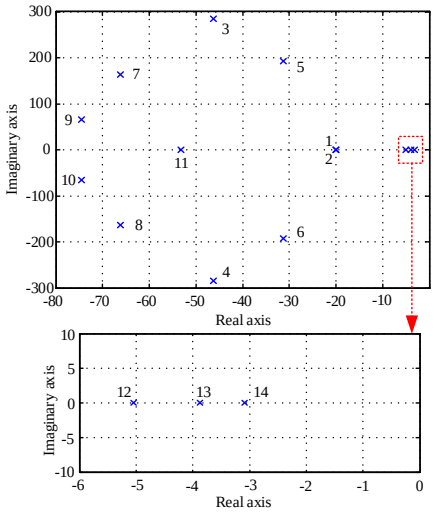

Fig. 6. Eigenvalue analysis of the four-terminal MTDC system.

C. Influence of Operating Conditions

In Fig. 7, the eigenvalue loci of the system with different operating conditions have been given. When P_{WF1} and P_{WF2} changing from 0.1p.u. to 1p.u., the MTDC system has enough stability margin, which indicates that the proposed control strategy performs well under different operating conditions.

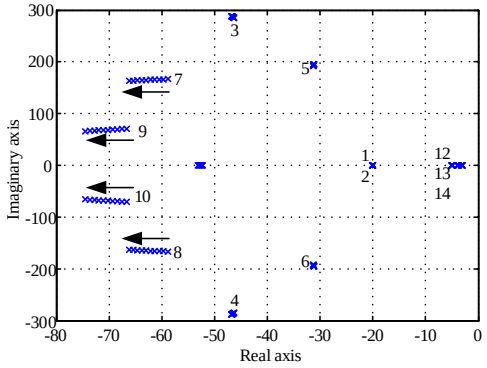

Fig. 7. Eigenvalue loci of the MTDC system with P_{WF1} and P_{WF2} changing from 0.1p.u. to 1p.u.

This conclusion will be verified in Section V-*A* by simulations of the proposed control strategy under different operating conditions.

D. Influence of Grid Stiffness

To figure out the influence of grid stiffness on system stability, the eigenvalue loci of the system when SCRs of both RECs vary from 10 to 2 are shown in Fig. 9.

It can be found that the eigenvalues 1, 2, 12, 13 and 14 keep

the same when SCR varies. The MTDC system still has enough stability margin even when RECs are connected to the very weak grid (SCR = 2). The proposed control strategy performs well under weak grid condition.

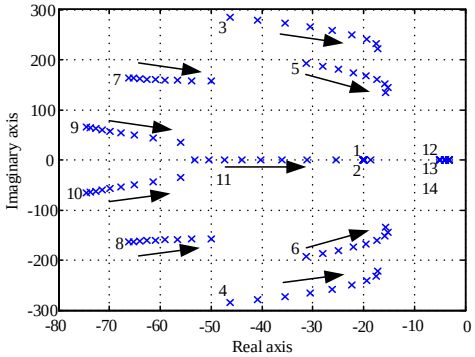

Fig. 8. Eigenvalue loci of the MTDC system with SCRs of both RECs changing from 10 to 2.

This conclusion will be verified in Section V-*B* by a comparative simulation study between the proposed control strategy and conventional control strategy under different grid conditions.

E. Influence of Control Coefficients

When designing the control coefficients, D_1/D_2, $K_1/(D_1+D_2)$ and $K_2/(D_1+D_2)$ should always keep the same. It is because that D_1/D_2 determines the steady-state power allocation between REC1 and REC2 (according to (11)), while $K_1/(D_1+D_2)$ and $K_2/(D_1+D_2)$ determine the primary frequency regulation coefficient of REC1 and REC2 (according to (16) and (17)). Therefore, when K_1 varies from 1 to 0.1, K_2, D_1 and D_2 should vary from 2 to 0.2, 1/30 to 1/300 and 1/60 to 1/600, respectively. Then Fig. 9 gives the eigenvalue loci of the MTDC system when K_1, K_2, D_1 and D_2 changes.

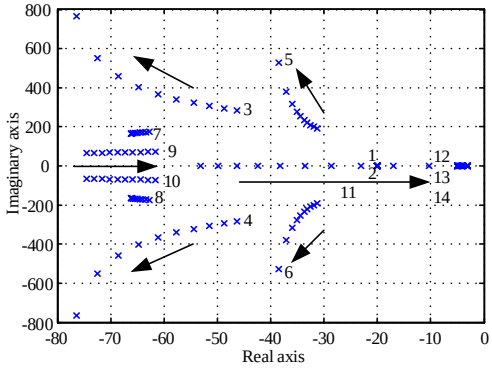

Fig. 9. Eigenvalue loci of the MTDC system with K_1, K_2, D_1 and D_2 changing from 1 to 0.1, 2 to 0.2, 1/30 to 1/300 and 1/60 to 1/600, respectively.

It can be observed that the MTDC system has acceptable stability margin during the variation of the control coefficients. More specifically, eigenvalues 3, 4, 5, 6 will move to the left, while the eigenvalues 7, 8, 9, 10, 11 will move to the right. The eigenvalues 1, 2, 12, 13, 14 will remain the same distribution. Among them, the eigenvalue 11 is the most critical. It moves towards the imaginary axis rapidly when K_1, K_2, D_1 and D_2 become smaller. This fact indicates that a larger K_1, K_2, D_1 and D_2 are beneficial to the system stability.

This conclusion will be verified in Section V-*A* by simulations of the proposed control strategy with different control coefficients.

F. Influence of Inertia Response from Wind Farm

It can be seen from Fig. 10 that eigenvalues 7~11 will move to the left with the increase of H_{WF}, while eigenvalues 12, 14, and 1~6 will stay the same. However, the eigenvalue 13 will move right and become the nearest pole from the imaginary axis. It means that the inertia response of wind farm may have negative effects on the stability of the MTDC system.

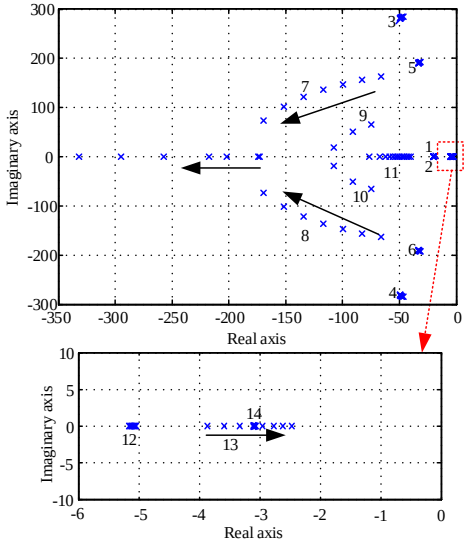

Fig. 10. Eigenvalue loci of the MTDC system with H_{WF1} and H_{WF2} changing from 1 to 10.

According to (21), the additional power ΔP_{add} is proportional to H_{WF}. If H_{WF} is too large, a small DC voltage ripple may lead to a large power variation of the wind farm. This power deviation will affect the DC voltage in turn according to (14). These interactions may reduce the stability margin of the system, or even lead to oscillations. Therefore, the virtual inertia H_{WF} should not be too large.

This conclusion will be verified in Section V-*A* by simulations of the proposed control strategy with different H_{WF}.

V. Simulation Analysis

In order to verify the effectiveness of the proposed control strategy, the Zhangbei project shown in Fig. 1 is built in PSCAD/MTDC. The AC grid is equivalent to a single SG. The capacities of Grid1 and Grid2 are 5GVA and 10GVA. Load1 and Load2 are 2GW and 4GW. The wind farm is equivalent to a single PMSG. The rated active power of WF1 and WF2 is 750MW and 1500MW. Other parameters are given in Table I. The single line diagram of the model is presented in Fig. 11. The reference direction of the active power of each terminal is also marked by the arrow.

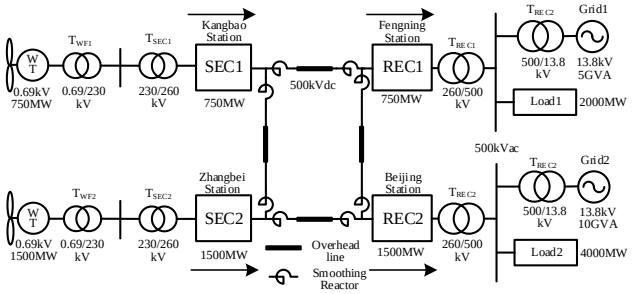

Fig. 11. Single line diagram of the simulated system.

A. *Simulation verification*

Case1: Influence of operating conditions

The control parameters K, D and H_{WF} are the same as Table II. Load 1 varies from 2GW to 2.5GW at t = 2s. Fig. 12 and 13 show the responses of wind farms and the MTDC system to the grid frequency variation under two different operating conditions:

1) P_{WF} =0.7p.u. (P_{WF1}= 500MW, P_{WF2} = 1000MW)

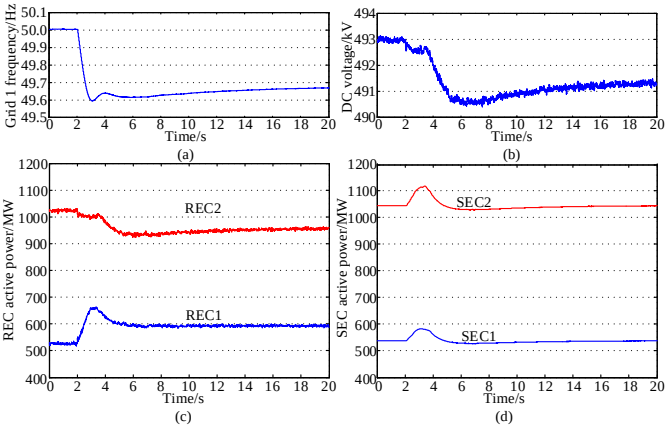

Fig. 12. Responses of wind farms and the MTDC system to grid frequency variation (P_{WF} =0.7p.u.)

2) P_{WF} = 0.2p.u. (P_{WF1}= 150MW, P_{WF2} = 300MW).

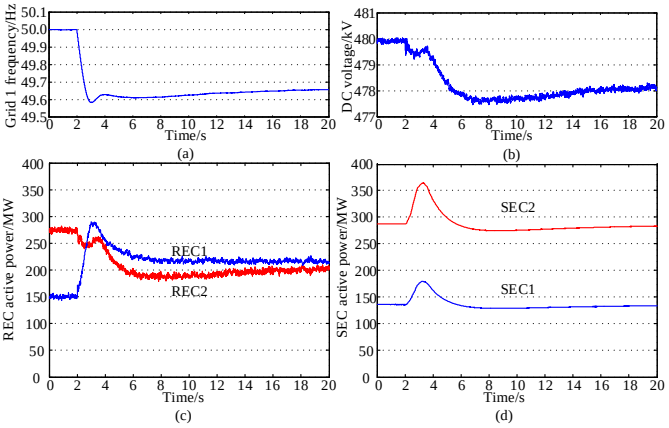

Fig. 13. Responses of wind farms and the MTDC system to grid frequency variation (P_{WF} =0.2p.u.)

It can be observed that the proposed control strategy performs well under different operating conditions. The DC voltage tracks the grid frequency variation autonomously. Both primary frequency regulation from REC2 and inertia response from wind farms are realized. Therefore, the effectiveness of the proposed control strategy under different operating conditions has been verified.

Case2: Influence of control coefficients

Fig. 14 shows the active power of REC1 and REC2 when the control coefficients K_1, K_2, D_1 and D_2 change.

It can be observed from Fig. 14 that the active power fluctuations of REC1 and REC2 are reduced with the increase of K and D, i.e., the system will have a larger damping ratio. Therefore, the analysis in Section IV-*E* is verified.

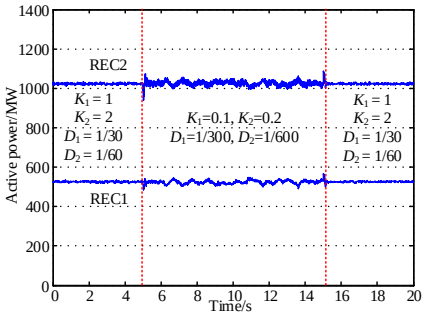

Fig. 14. Active power of the REC1 and REC2 with different values of K_1, K_2, D_1 and D_2

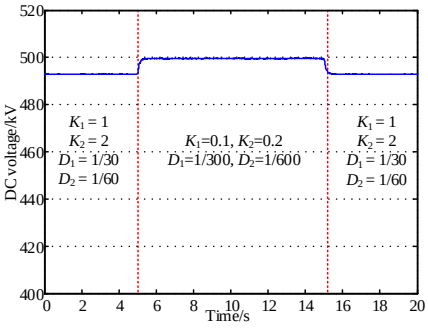

Fig. 15. DC voltage with different values of K_1, K_2, D_1 and D_2

In addition, equation (14) indicates that the steady-state deviation of the DC voltage is proportional to both P_{WF} - P_{ref} and 1/ $(1/D_1+1/D_2)$, which has been proven in Fig. 15. Therefore, K and D cannot be too large, otherwise, the steady-state DC voltage deviation may exceed the limitation (±5%).

Case3: Influence of Inertia Response from Wind Farm

Figs. 16 and 17 show the active power of SEC1 and SEC2 and DC voltage with different virtual inertia H_{WF1} and H_{WF2}.

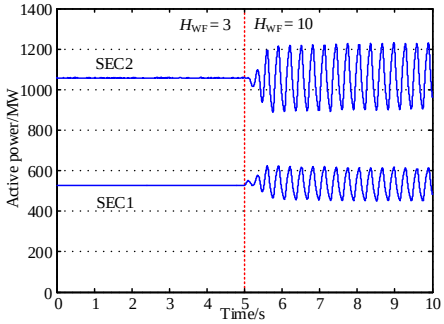

Fig. 16. DC voltage with different values of H_{WF}

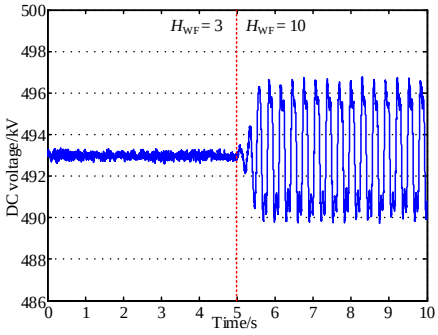

Fig. 17. Active power of the REC1 and REC2 with different values of H_{WF}

The output power of SECs and DC voltage start to oscillate when the virtual inertia of the wind farm H_{WF} is changed to 10 at t = 5s, which proves the analysis in Section IV-*F*.

B. Comparative study of proposed and conventional control

This section will compare the frequency response and weak grid operation capability of the MTDC system using the proposed control and conventional control strategies, they are:

PC (proposed control) is the proposed control strategy in this paper. The control parameters *K*, *D* and H_{WF} are in Table II.

CC (conventional control) is the conventional PLL-based vector control strategy without ancillary frequency response control. The bandwidths of its PLL, DC voltage loop and inner current loop are 50Hz, 20Hz and 200Hz, respectively.

CCFR (conventional control with ancillary frequency response control [7]). The ancillary frequency response is achieved by the U_{DC}-*f* droop control of RECs, where the grid frequency deviation is usually detected by PLL.

Case1: Performance under Stiff Grids

The SCRs of REC 1 and 2 are 7.5, which stands for a stiff grid. Load 1 varies from 2GW to 2.5GW at t = 2s. The simulation results are shown in Fig. 18.

It can be observed that with the control of CCFR and PC, the DC voltage tracks the variation of grid frequency [see Fig. 18(a) and (b)]. The power flow of the DC grid is autonomously changed. REC2 reduces its active power to provide primary frequency regulation to Grid 1 [see Fig. 18(d)]. Then the wind farms are informed with the grid frequency deviation and provide inertia response [see Fig. 18(e) and (f)]. The output active power of REC1 is shown in Fig. 18(c). Compared with the CC, the minimum grid frequency of the CCFR and PC is increased by 0.1Hz [see Fig. 18(b)]. These simulation results prove that both control strategies perform well under stiff grid conditions.

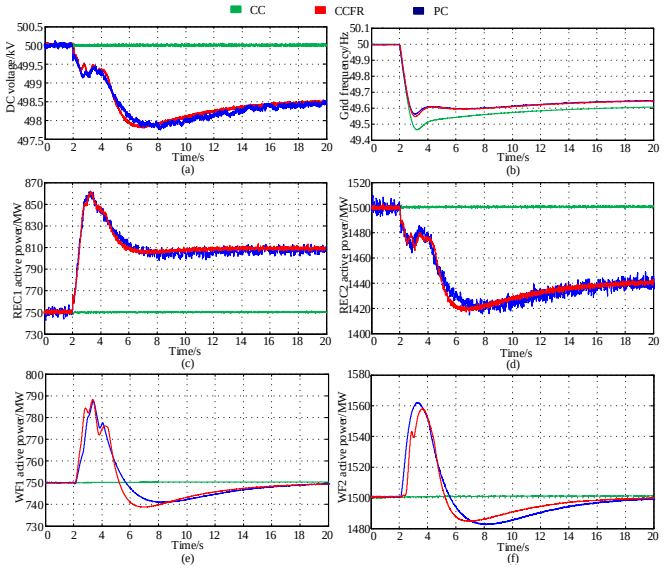

Fig. 18. Responses of wind farms and the MTDC system with CC, CCFR, and PC in Case1.

Case2: Performance under Weak Grids

The SCR of REC1 is 2.5, which stands for a weak grid. The SCR of REC2 is 7.5, which stands for a stiff grid. Load 1 varies from 2GW to 1.5GW at t = 2s.

The performance of CC and CCFR is shown in Fig. 19. The active power of REC1 starts to oscillate with the decrease of the SCR. It can be seen that the CC and CCFR methods, which are based on PLL and current-vector control, are unstable under this weak grid condition.

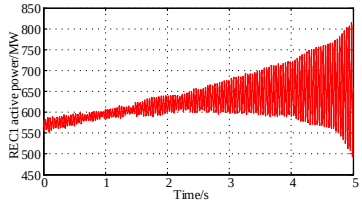

Fig. 19. Active power of REC1 with the CC and CCFR control in Case 2

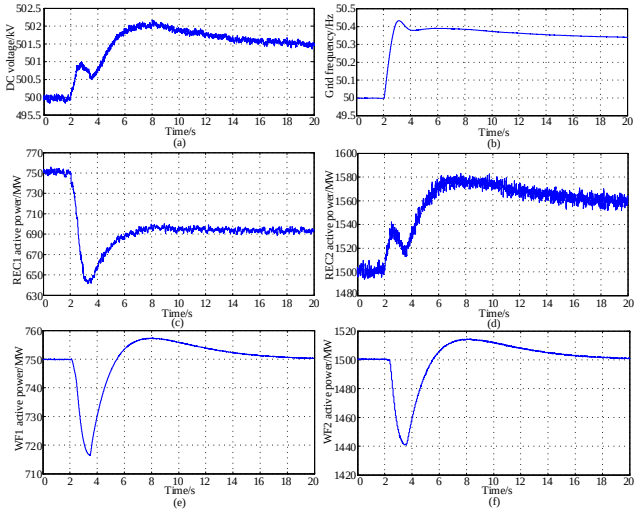

Fig. 20. Responses of wind farms and the MTDC system with PC in Case2.

In contrast, the PC still performs well even under weak grid conditions. The power allocation in the DC grid will change when the load suddenly decreases and grid frequency starts to increase [see Fig. 20 (b)]. REC2 increases its active power [see

Fig. 20 (d)]. The DC voltage increases, thus helping the wind farms to realize inertia responses [see Fig. 20 (a), (e) and (f)]. These simulation results prove that the PC has better performance when the MTDC connects to weak grids. The comparison of simulation results in Case 1 and Case 2 verifies the analysis in Section IV-*D*.

VI. Conclusion

This paper presents an autonomous grid-synchronizing and frequency response control of an MTDC system with wind farm integration. Comparative simulation studies on a practical Zhangbei four-terminal DC system (China) indicate two significant advantages of the proposed method over the conventional one (PLL-based vector control), which are:

1) The frequency response among the AC systems can be achieved in an autonomous manner, which is fast and communication free;

2) RECs with the proposed control method can work stably even under very weak AC grid conditions.

In addition, the small-signal stability of the overall system is evaluated by eigenvalue analysis. Influences of the droop coefficient D, the coupling coefficient K and the virtual inertia H_{WF} of the wind farms, are analyzed. The obtained results are useful guidelines for the stability-oriented parameter tuning.

References

[1] G. Li, *et al*, "Feasibility and reliability analysis of LCC DC grids and LCC/VSC hybrid DC grids," *IEEE Access*, vol. 7, pp. 22445-22456, Feb. 2019.

[2] N. Flourentzou, V. G. Agelidis and G. D. Demetriades, "VSC-Based HVDC Power Transmission Systems: An Overview," in *IEEE Transactions on Power Electronics*, vol. 24, no. 3, pp. 592-602, March 2009.

[3] S. M. Muyeen, R. Takahashi and J. Tamura, "Operation and Control of HVDC-Connected Offshore Wind Farm," in *IEEE Transactions on Sustainable Energy*, vol. 1, no. 1, pp. 30-37, April 2010.

[4] K. Sun et al., "VSC-MTDC System Integrating Offshore Wind Farms Based Optimal Distribution Method for Financial Improvement on Wind Producers," in *IEEE Transactions on Industry Applications*, vol. 55, no. 3, pp. 2232-2240, May-June 2019.

[5] L. M. Castro and E. Acha, "On the Provision of Frequency Regulation in Low Inertia AC Grids Using HVDC Systems," in *IEEE Transactions on Smart Grid*, vol. 7, no. 6, pp. 2680-2690, Nov. 2016.

[6] F. D. Bianchi and J. L. Domnguez-Garca, "Coordinated Frequency Control Using MT-HVDC Grids With Wind Power Plants," in *IEEE Transactions on Sustainable Energy*, vol. 7, no. 1, pp. 213-220, Jan. 2016.

[7] B. Silva, C. L. Moreira, L. Seca, Y. Phulpin and J. A. Pecas Lopes, "Provision of Inertial and Primary Frequency Control Services Using Offshore Multiterminal HVDC Networks," in *IEEE Transactions on Sustainable Energy*, vol. 3, no. 4, pp. 800-808, Oct. 2012.

[8] Y. Phulpin, "Communication-Free Inertia and Frequency Control for Wind Generators Connected by an HVDC-Link," in *IEEE Transactions on Power Systems*, vol. 27, no. 2, pp. 1136-1137, May 2012.

[9] N. R. Chaudhuri, R. Majumder and B. Chaudhuri, "System Frequency Support Through Multi-Terminal DC (MTDC) Grids," in *IEEE Transactions on Power Systems*, vol. 28, no. 1, pp. 347-356, Feb. 2013.

[10] O. D. Adeuyi, M. Cheah-Mane, J. Liang and N. Jenkins, "Fast Frequency Response From Offshore Multiterminal VSC–HVDC Schemes," in *IEEE Transactions on Power Delivery*, vol. 32, no. 6, pp. 2442-2452, Dec. 2017.

[11] C. Zhang, X. Cai, A. Rygg and M. Molinas, "Sequence Domain SISO Equivalent Models of a Grid-Tied Voltage Source Converter System for Small-Signal Stability Analysis," in *IEEE Transactions on Energy Conversion*, vol. 33, no. 2, pp. 741-749, June 2018.

[12] J. Lyu, X. Zhang, X. Cai and M. Molinas, "Harmonic State-Space Based Small-Signal Impedance Modeling of a Modular Multilevel Converter With Consideration of Internal Harmonic Dynamics," in *IEEE Transactions on Power Electronics*, vol. 34, no. 3, pp. 2134-2148, March 2019.

[13] D. Dong, B. Wen, D. Boroyevich, P. Mattavelli and Y. Xue, "Analysis of Phase-Locked Loop Low-Frequency Stability in Three-Phase Grid-Connected Power Converters Considering Impedance Interactions," in *IEEE Transactions on Industrial Electronics*, vol. 62, no. 1, pp. 310-321, Jan. 2015.

[14] B. Wen, D. Dong, D. Boroyevich, R. Burgos, P. Mattavelli and Z. Shen, "Impedance-Based Analysis of Grid-Synchronization Stability for Three-Phase Paralleled Converters," in *IEEE Transactions on Power Electronics*, vol. 31, no. 1, pp. 26-38, Jan. 2016.

[15] J. Driesen and K. Visscher, "Virtual synchronous generators," 2008 IEEE Power and Energy Society General Meeting - Conversion and Delivery of Electrical Energy in the 21st Century, Pittsburgh, PA, 2008, pp. 1-3.

[16] Q. Zhong and G. Weiss, "Synchronverters: Inverters That Mimic Synchronous Generators," in *IEEE Transactions on Industrial Electronics*, vol. 58, no. 4, pp. 1259-1267, April 2011.

[17] Y. Cao et al., "A Virtual Synchronous Generator Control Strategy for VSC-MTDC Systems," in *IEEE Transactions on Energy Conversion*, vol. 33, no. 2, pp. 750-761, June 2018.

[18] J. He, K. Wu, L. Huang, H. Xin, C. Lu and H. Wang, "A Coordinated Control Scheme to Realize Frequency Support of PMSG-Based Wind Turbines in Weak Grids," 2018 IEEE Power & Energy Society General Meeting (PESGM), Portland, OR, 2018, pp. 1-5.

[19] I. Cvetkovic, D. Boroyevich, R. Burgos, C. Li, M. Jaksic, P. Mattavelli, "Modeling of a virtual synchronous machine-based grid-interface converter for renewable energy systems integration", *Proc. IEEE* 15th Workshop Control Modeling Power Electron. (COMPEL), pp. 1-7, Jun. 2014.

[20] L. Huang et al., "A Virtual Synchronous Control for Voltage-Source Converters Utilizing Dynamics of DC-Link Capacitor to Realize Self-Synchronization," in *IEEE Journal of Emerging and Selected Topics in Power Electronics*, vol. 5, no. 4, pp. 1565-1577, Dec. 2017.

[21] R. Yang, C. Zhang, X. Cai and G. Shi, "Autonomous grid-synchronising control of VSC-HVDC with real-time frequency mirroring capability for wind farm integration," in *IET Renewable Power Generation*, vol. 12, no. 13, pp. 1572-1580, 2018.

[22] J. Morren, S. W. H. de Haan, W. L. Kling and J. A. Ferreira, "Wind turbines emulating inertia and supporting primary frequency control," in *IEEE Transactions on Power Systems*, vol. 21, no. 1, pp. 433-434, Feb. 2006.

[23] J. Lee, E. Muljadi, P. Srensen and Y. C. Kang, "Releasable Kinetic Energy-Based Inertial Control of a DFIG Wind Power Plant," in *IEEE Transactions on Sustainable Energy*, vol. 7, no. 1, pp. 279-288, Jan. 2016.

[24] J. M. Mauricio, A. Marano, A. Gomez-Exposito and J. L. Martinez Ramos, "Frequency Regulation Contribution Through Variable-Speed Wind Energy Conversion Systems," in *IEEE Transactions on Power Systems*, vol. 24, no. 1, pp. 173-180, Feb. 2009.

Renxin Yang (S'19) received the B.Eng degree in electrical engineering and automation from Huazhong University of Science and Technology, Wuhan, China, in 2014. Since September 2014, he has been working towards the Ph.D degree in Wind Power Research Center, Shanghai Jiao Tong University. His current research interests include topology, control, active frequency response and fault ride-through of MMC-based HVDC system with wind farm integration.

Gang Shi (S'13-M'15) received the B.Eng., M.Sc., and Ph.D. degrees in electrical engineering from Shanghai Jiao Tong University, Shanghai, China, in 2007, 2009, and 2014, respectively. He was as a Research Fellow with the School of Engineering, Aberdeen University, U.K., in 2015 and with the School of Electronic Electrical and Systems Engineering, University of Birmingham, U.K., from 2017 to 2018. He is currently an Assistant Professor with the Wind Power Research Center, Shanghai Jiao Tong University. His current research interests include topology, operation, and control of dc grid for offshore wind power collection and transmission, and modeling and control of key components in the dc grid.

Xu Cai received the B.Eng. degree from Southeast University, Nanjing, China, in 1983, and the M.Sc. and Ph.D. degrees from the China University of Mining and Technology, Xuzhou, China, in 1988 and 2000, respectively. He was with the Department of Electrical Engineering, China University of Mining and Technology, as an Associate Professor from 1989 to 2001. He was the Vice Director of the State Energy Smart Grid R&D Center, Shanghai, China, from 2010 to 2013. He has been with Shanghai Jiao Tong University, Shanghai, as a Professor since 2002, where he has also been the Director of the Wind Power Research Center since 2008. His current research interests include power electronics and renewable energy exploitation and utilization, including wind power converters, wind turbine control system, large power battery storage systems, clustering of wind farms and its control system, and grid integration.

Chen Zhang received the B.Eng. degree from the China University of Mining and Technology, China, and the Ph.D. from Shanghai Jiao Tong University, China, in 2011 and 2018 respectively. He was a Ph.D. Visiting Scholar with the Department of Engineering Cybernetics, Norwegian University of Science and Technology, Norway, in 2015. Currently, he is a Postdoctoral Research Fellow at NTNU. His research interest is modeling and stability analysis of VSC-based energy conversion systems, where the aim is to reveal the fundamental dynamics and stability mechanisms of renewable energies with VSCs as the grid interface.

Gen Li (M'18) received the B.Eng. degree in Electrical Engineering and its Automation from Northeast Electric Power University, Jilin, China, in 2011, the M.Sc. degree in Power Engineering from Nanyang Technological University, Singapore, in 2013 and the Ph.D. degree in Electrical Engineering from Cardiff University, Cardiff, U.K., in 2018.

From 2013 to 2016, he was a Marie Curie Early Stage Research Fellow funded by the European Union's MEDOW project. He has been a Visiting Researcher at China Electric Power Research Institute and Global Energy Interconnection Research Institute, Beijing, China, at Elia, Brussels, Belgium and at Toshiba International (Europe), London, U.K. He has been a Research Associate at the School of Engineering, Cardiff University since 2017. His research interests include control and protection of HVDC and MVDC technologies, power electronics, reliability modelling and evaluation of power electronics systems.

Dr. Li is a Chartered Engineering in the U.K. He is an Associate Editor of the CSEE Journal of Power and Energy Systems. His Ph.D. thesis received the First CIGRE Thesis Award in 2018.

Jun Liang (M'02-SM'12) received the B.Sc. degree in Electric Power System & its Automation from Huazhong University of Science and Technology, Wuhan, China, in 1992 and the M.Sc. and Ph.D. degrees in Electric Power System & its Automation from the China Electric Power Research Institute (CEPRI), Beijing, in 1995 and 1998, respectively.

From 1998 to 2001, he was a Senior Engineer with CEPRI. From 2001 to 2005, he was a Research Associate with Imperial College London, U.K.. From 2005 to 2007, he was with the University of Glamorgan as a Senior Lecturer. He is currently a Professor in Power Electronics with the School of Engineering, Cardiff University, Cardiff, U.K. He is a Fellow of the Institution of Engineering and Technology (IET). He is the Chair of IEEE UK and Ireland Power Electronics Chapter. He is an Editorial Board Member of CSEE JPES. He is the Coordinator and Scientist-in-Charge of two European Commission Marie-Curie Action ITN/ETN projects: MEDOW (€3.9M) and InnoDC (€3.9M). His research interests include HVDC, MVDC, FACTS, power system stability control, power electronics, and renewable power generation.